

# Attenuated immune surveillance during squamous cell transformation of pancreatic adenosquamous cancer defines new therapeutic opportunity for cancer interception

Xinyuan Chen <sup>1,2</sup>, Shanyue Sun,<sup>3</sup> Shuofeng Li <sup>4</sup>, Shuangni Yu,<sup>1,2</sup>  
Jie Chen <sup>1,2</sup>, Xianlong Chen<sup>1,2</sup>

**To cite:** Chen X, Sun S, Li S, *et al.* Attenuated immune surveillance during squamous cell transformation of pancreatic adenosquamous cancer defines new therapeutic opportunity for cancer interception. *Journal for ImmunoTherapy of Cancer* 2025;**13**:e012066. doi:10.1136/jitc-2025-012066

► Additional supplemental material is published online only. To view, please visit the journal online (<https://doi.org/10.1136/jitc-2025-012066>).

Accepted 11 June 2025



© Author(s) (or their employer(s)) 2025. Re-use permitted under CC BY-NC. No commercial re-use. See rights and permissions. Published by BMJ Group.

<sup>1</sup>Department of Pathology, Peking Union Medical College Hospital, Beijing, Beijing, China

<sup>2</sup>Key Laboratory of Research in Pancreatic Tumor, Chinese Academy of Medical Sciences and Peking Union Medical College, Beijing, Beijing, China

<sup>3</sup>Shandong Provincial Hospital Affiliated to Shandong First Medical University, Jinan, Shandong, China

<sup>4</sup>Department of Liver Surgery, Peking Union Medical College Hospital, Beijing, Beijing, China

## Correspondence to

Xianlong Chen;  
xlchen1995@sina.com

## ABSTRACT

**Background** Pancreatic adenosquamous cancer (PASC) is an extremely rare subtype of pancreatic cancer characterized by a poorer prognosis and higher likelihood of metastasis compared with the more prevalent pancreatic ductal adenocarcinoma (PDAC). Although genomic changes during PASC tumorigenesis have been documented, the corresponding alterations in the tumor immune microenvironment (TIME) remain inadequately elucidated. Therefore, this study aims to analyze the immune landscape of PASC by employing multiplex immunohistochemistry (mIHC) and digital image analysis.

**Methods** In this study, we analyzed four independent cohorts comprising 120 patients with PASC and 386 patients with PDAC. We employed mIHC to quantify three in situ panels of immuno-oncology-related biomarkers at subcellular resolution. We then used five samples to perform laser capture microdissection, RNA sequencing, and whole-exome sequencing to explore the underlying mechanisms of the compartment-specific immune phenotypes in PASC.

**Results** Our findings revealed a more immunosuppressive TIME in PASC compared with PDAC, characterized by a decreased abundance of T cells. Immune cell types indicative of enhanced immune surveillance, including cytotoxic and memory T cells and antigen-experienced T cells, were present at significantly lower densities in PASC compared with PDAC. Conversely, some immunosuppressive macrophage phenotypes exhibited increased distribution in PASC. Immunosuppressive immune cells (ICs) were abundant, enriched within stromal regions, highly heterogeneous across tumors, and exhibited distinct distributions between squamous cell (SQC) and adenocarcinoma (ADC) compartments in PASC. Notably, the TIME of SQC compartments harbored more exhausted T cells compared with synchronous ADC compartments, indicating attenuated immune surveillance during squamous transformation. Transcriptomic profiling of microdissected SQC and ADC regions revealed immune exhaustion signatures and downregulated T-cell differentiation pathways in SQC compartments, alongside altered antigen presentation machinery and elevated tumor mutational burden, suggesting squamous-specific tumor-associated antigens with potential

## WHAT IS ALREADY KNOWN ON THIS TOPIC

⇒ Pancreatic adenosquamous cancer (PASC) was an extremely rare and aggressive malignancy in pancreatic cancer, exhibiting high resistance to multiple therapies. Several studies based on a limited number of patients with PASC demonstrated the genomic alteration during tumorigenesis. However, the tumor immune microenvironment (TIME) remains inadequately elucidated.

## WHAT THIS STUDY ADDS

⇒ Based on four independent cohorts, this study characterized and validated the immune profiles of PASC, indicating a suppressive TIME of PASC. Highly intra-immune/inter-immune heterogeneity was also identified across tumors, epithelial/stromal areas, and squamous cell/adenocarcinoma compartments in PASC. Not only the densities but also the spatial proximity of TIGIT<sup>+</sup>CD8<sup>+</sup> T cells and CD155<sup>+</sup>CD68<sup>+</sup>macrophages to tumor cells are associated with patient outcomes, highlighting the potential role of spatially resolved immune cell subtypes as quantitative biomarkers for PASC prognosis and therapy. Moreover, we found that distinct expression patterns of the programmed cell death protein-1 (PD-1)/programmed death ligand 1 (PD-L1) and T-cell immunoreceptor with immunoglobulin and the ITIM domain (TIGIT)/CD155 axes in the PASC TIME associated with survival outcomes.

## HOW THIS STUDY MIGHT AFFECT RESEARCH, PRACTICE OR POLICY

⇒ The findings suggested that the suppressive TIME and immune heterogeneity might contribute to the inferior survival outcomes and malignant phenotypes in the patients with PASC. Moreover, we underscored the potential of targeting immune checkpoint pathways, such as the TIGIT/CD155 and PD-1/PD-L1 axes, as a therapeutic strategy for PASC.

immunotherapeutic relevance. Beyond differences in IC density, we observed closer spatial proximity of CD45RO<sup>+</sup> and PD-1<sup>+</sup>CD3<sup>+</sup>CD8<sup>+</sup> T cells to tumor cells within 10,

20 and 30  $\mu\text{m}$  ranges in PASC compared with PDAC, with variations by histological subregion. Furthermore, we found distinct expression patterns of the programmed cell death protein-1 (PD-1)/programmed death ligand 1 (PD-L1) and T-cell immunoreceptor with immunoglobulin and the ITIM domain (TIGIT)/CD155 axes in the PASC TIME associated with survival outcomes. Notably, TIGIT<sup>+</sup>CD8<sup>+</sup> T cells and CD155<sup>+</sup> CD68<sup>+</sup> macrophages, along with their proximity to tumor cells, served as independent prognostic indicators. These findings were validated in an independent cohort study.

**Conclusion** Our study advances the understanding of PASC by providing updated insights into its immunoenvironmental features. These findings underscore the potential of targeting immune checkpoint pathways, particularly the TIGIT/CD155 and PD-1/PD-L1 axes, as a therapeutic strategy for PASC.

## INTRODUCTION

Pancreatic cancer (PC) remains one of the most lethal malignancies worldwide, with a 5-year survival rate of less than 10% and approximately 50,000 deaths annually.<sup>1</sup> Among its subtypes, pancreatic adenosquamous carcinoma (PASC), a rare and highly aggressive histological subtype characterized by the coexistence of ductal adenocarcinoma (ADC) and squamous cell carcinoma (SQC) components, with SQC components constituting more than 30% of the tumor. PASC accounts for 0.5–4% of all PC cases.<sup>2–4</sup> Compared with pancreatic ductal adenocarcinoma (PDAC), the most prevalent subtype of PC, PASC exhibits a higher metastatic potential and worse clinical outcome.<sup>3–5</sup> However, an extensive population-based analysis found no significant difference in tumor stage at diagnosis between PDAC and PASC. Surgical resection and conventional chemotherapy regimens, including gemcitabine, nab-paclitaxel, and FOLFIRINOX, have demonstrated limited efficacy in PASC.<sup>6,7</sup> Several theories exist regarding the presence of this histological subtype, given that the normal pancreatic tissue lacks a benign squamous epithelium. These include the formation of a squamous epithelium triggered by inflammation, convergence of different tumor lineages within the same tissue, and abnormal differentiation and enrichment of stem cells that adopt traits of one or both subtypes. Due to the rarity of PASC and the lack of preclinical models, its tumorigenesis, progression, and immune-microenvironmental characteristics remain unclear. Consequently, no immunotherapy or targeted therapy is currently available for PASC.

Next-generation sequencing has identified various somatic genomic lesions targeting chromatin regulators in PASC genomes, which are superimposed on well-characterized genomic lesions commonly found in PDAC. These include mutations in *KRAS* and *TP53*, homozygous deletion of *CDKN2A*, and amplification of *MYC*. Additionally, PASC exhibits a higher frequency of mutations in *TP53*, *KRAS2*, *UPFI*, and chromosome 3p compared with PDAC,<sup>6,7</sup> highlighting distinct genetic alterations during tumorigenesis. Notably, a recent study revealed that the ADC and SQC compartments of PASC shared a similar genomic landscape, suggesting that both

compartments may originate from the same progenitor lesion.<sup>8</sup> Unlike melanoma or lung cancers, PDAC is primarily an immunologically “cold” cancer, rendering it largely resistant to immunotherapy.<sup>9,10</sup> Research on the immune profiling of the PDAC tumor immune microenvironment (TIME) has revealed a complex network of immunosuppressive cellular and cytokine interactions, contributing to the minimal efficacy of immune checkpoint inhibitors.<sup>11</sup> In contrast, a previous study reported that PASC also referred to as “quasimesenchymal” or “basal-like”, exhibited an immune escape phenotype; however, this finding was based on a cohort with a very small sample size. Furthermore, a recent study suggests that immunosuppressive pathways, including the downregulation of B-cell activation and immune responses, are enriched in cancer-associated fibroblasts of PASC.<sup>8</sup> Using single-cell RNA sequencing in a single PASC case, Zhao *et al* identified the *C5ARI/RPS19* axis as a key driver of CD8<sup>+</sup> T-cell depletion and regulatory T cell (Treg) expansion.<sup>12</sup> Their communication analyses between myeloid and cancer cells suggest that immune modulation plays a crucial role in PASC progression. These findings highlight the complexity of the TIME and underscore the need for a comprehensive spatial analysis of PASC. In light of these observations, a deeper understanding of the immune microenvironment of PASC is essential to elucidate the role of innate and adaptive immunity during its multistep progression. Nonetheless, an in-depth, high-dimensional exploration of the PASC TIME, including a separate assessment of isolated SQC compartments versus those with synchronous ADC compartments or PDAC, has not been conducted. Such an analysis could provide unprecedented insights and potentially open a therapeutic window for immune interception in PASC.

The advent of immunotherapy targeting programmed death ligand 1 (PD-L1) marked a new era in cancer treatment. By blocking the programmed cell death protein-1 (PD-1)/PD-L1 pathway, T cells are reactivated, leading to cancer regression. Additionally, the T-cell immunoreceptor with immunoglobulin and the ITIM domain (TIGIT), an inhibitory receptor expressed on effector T cells, Tregs, and natural killer (NK) cells, plays a crucial role in modulating both innate and adaptive immunity.<sup>13,14</sup> Together with its specific ligand CD155, the TIGIT/CD155 axis promotes T-cell exhaustion by downregulating interleukin (IL)-12 and upregulating IL-10 secretion, further contributing to immune evasion.<sup>15,16</sup> Given the potential clinical relevance of these immune checkpoints, both the PD-1/PD-L1 and TIGIT/CD155 axes represent promising therapeutic targets.<sup>17</sup> For instance, a phase II clinical study (NCT03563716) demonstrated an improved objective response rate (ORR) of 31.3% in patients with non-small cell lung cancer receiving anti-TIGIT plus anti-PD-1 therapy, compared with an ORR of 16.2% in those treated with anti-PD-1 alone.<sup>18</sup> However, due to the rarity of PASC, the role of immune checkpoint expression in the TME and its clinical implications, particularly its

impacts on related immunotherapy efficacy, remain inadequately explored.

In this study, we aimed to characterize the immune profiles of PASC, including a separate assessment of isolated SQC compartments versus those with synchronous ADC compartments or PDAC, by integrating multiplex immunohistochemistry (mIHC) and digital image analysis. Using four independent retrospective clinical cohorts, including two PASC and two PDAC cohorts, we explored the spatial organization of tumors and immune cells (ICs) and assessed their clinical significance. Additionally, we investigated the expression patterns of immune checkpoint molecules, including the PD-1/PD-L1 and TIGIT/CD155 axes, in both tumor and ICs to provide valuable insights for the future development of immunotherapeutic strategies for PASC.

## METHODS

### Patients and specimens

In this study, a training set of 92 formalin-fixed paraffin-embedded (FFPE) PASC tissue samples and 291 FFPE PDAC samples from Peking Union Medical College (PUMCH) were analyzed, along with a validation set of 28 PASC samples and 95 PDAC samples from Shandong Provincial Hospital. The study was conducted in accordance with the Declaration of Helsinki. Written informed consent was obtained from all participants. All tissue samples were obtained from patients who underwent surgery without neoadjuvant therapy. According to the 2019 WHO classification of digestive system tumors, PASC samples in this study were defined as having at least 30% squamous differentiation. All pathological slides were reviewed by two expert PC pathologists (SY and JC).

Clinicopathological data, including patient age, sex, preoperative serum carbohydrate antigen 19-9 (CA19-9) levels, tumor location, tumor size, T stage, N stage, American Joint Committee on Cancer (AJCC) stage, administration of adjuvant chemotherapy, tumor differentiation, perineural invasion (PNI), lymphovascular invasion (LVI), and follow-up information, were available for all cases (online supplemental tables 1 and 2). Progression-free survival (PFS) and overall survival (OS) were calculated from the date of surgery to the date of progression, death, or last follow-up.

For each sample, FFPE tissue blocks containing the highest proportions of SQC and ADC components within the lesion were selected. The blocks were sliced into consecutive serial sections, each 4mm thick. The slides were stained using three multiple immunofluorescence (mIF) panels and traditional single IHC.

### Identification of regions of interest for digital image analysis

Distinct histopathological features in H&E-stained tissue sections were selected as regions of interest (ROI) for conventional IHC and mIHC analyses. The H&E-stained samples were digitized at 20× magnification with a Hamamatsu S60 whole-slide scanner (Hamamatsu Photonics,

Hamamatsu City, Japan), and the images were examined with NanoZoomer Digital Pathology view2 software (V.2.7.25, Hamamatsu Photonics). The SQC and ADC compartments, as well as PDAC, were identified and annotated. We selected approximately five non-overlapping ROIs from both the SQC and ADC compartments for each case (detailed information about the number of ROIs analyzed in each compartment is shown in online supplemental table 3).

### Evaluation of TLS

Tertiary lymphoid structures (TLS) were identified as ectopic lymphoid structures with lymphoid cells aggregated that lacked integrated organized structures such as capsules. In our study, TLS was morphologically detected using H&E-stained images via an automated pipeline (<https://github.com/YuMeng-W/TumSeg-main>), which achieved a good agreement with manual TLS counting by pathologists using digital H&E-stained images. TLS density was calculated as number/mm<sup>2</sup> in the tumorous and peritumoral region (defined as 5 mm from the infiltrative tumor border). We also measured the nearest distance of the lymphoid aggregates to SQC or ADC epithelium.

### Immunohistochemistry

Immunohistochemical staining was performed using an automated immunostainer (BOND-III; Leica Biosystems, Wetzlar, Germany) following the manufacturer's standard protocols. Details of the primary antibodies used for staining are listed in online supplemental table 4.

### Multiplex immunohistochemistry and multispectral imaging

The multiplex fluorescence staining was performed using the Opal Polaris 7-color kit (Akoya Biosciences) according to the manufacturer's instructions. The representative mIHC images and corresponding conventional IHC images were exhibited in [figure 1A–C](#). Multiplex-stained sections were imaged using the Vectra Polaris system (Vectra 3.0 system; Akoya Biosciences), which establishes an image cube by capturing the fluorescent spectra at 20 nm wavelength intervals from 420 to 720 nm. The stained sections were scanned concurrently using a Vectra multispectral slide scanner (Vectra 3.0; PerkinElmer). InForm image analysis software (Akoya Biosciences) was used for spectral unmixing through a library established based on each primary antibody-TSA fluorophore combination to provide references for cell phenotypes. Detailed procedures are provided in online supplemental table 4 and methods.

The pathologists (XinC and XiaC) conducting the analyses chose the ROIs (930×700 μm), based on the histopathologic features observed in H&E-stained slides, after consultation with two expert PC pathologists (SY and JC). For digital imaging analysis, the ROIs were scanned at 20× resolution using InForm V.2.4 software (Akoya Biosciences), which offers a user-trainable algorithm for tissue segmentation based on morphology and specific

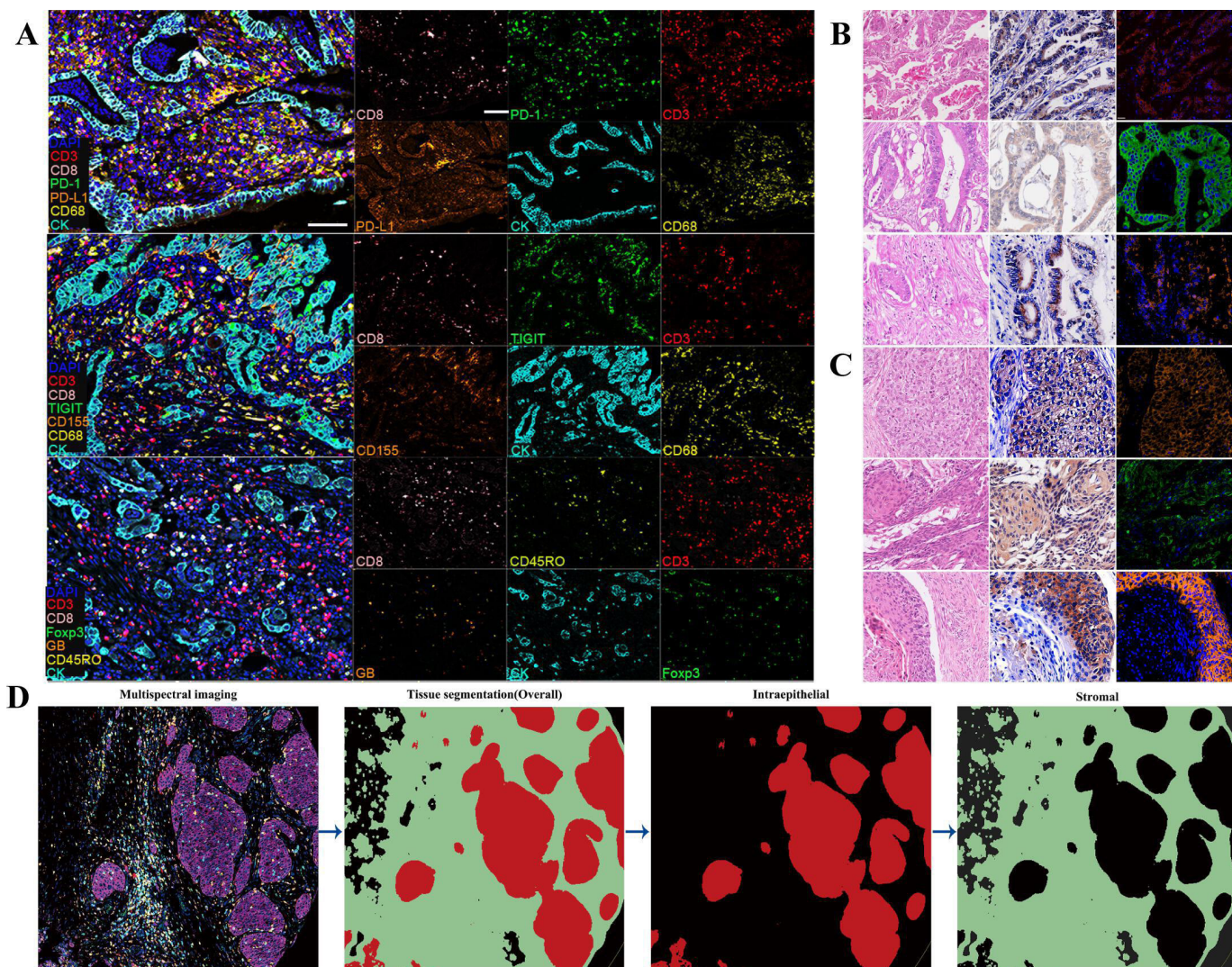


**Figure 1** Multiplex immunohistochemistry and image analysis pipeline for immune profiling of pancreatic adenosquamous carcinoma (PASC). (A) Representative composite and single-stained images of the multiplex immunohistochemistry panels used. (B–C) Comparison of staining patterns among H&E, chromogenic immunohistochemistry, and multiple immunofluorescence of CD155, TIGIT, and PD-L1 revealed comparable staining patterns in both adenocarcinoma (B) and squamous cell (C) compartments of PASC. (D) Overview of the automated image analysis pipeline. Scale bar: 200  $\mu$ m. PD-L1, programmed death (ligand) 1; TIGIT, T-cell immunoreceptor with immunoglobulin and the ITIM domain.

markers (figure 1D). Details of cell segmentation are listed in online supplemental methods and table 5. Each ROI was classified into two compartments: the intraepithelial compartment, defined as an area with cancer cells, including ICs in between the epithelial cells or the stroma in contact with the basal membrane, and the stromal compartment, represented by the stroma tissue adjacent to the carcinoma compartment, including ICs that are not in contact with the basal membrane. In this study, the following markers were evaluated in panel 1: PD-L1, PD-1, CD3, CD8, CD68, CK, and DAPI, the second panel included CD155, TIGIT, CD3, CD8, CD68, CK, and DAPI, while the third panel included CD3, CD4, CD8, GrB (granzyme B), CD45RO, FOXP3, and DAPI. All IC phenotypes are summarized in online supplemental table 6.

### Evaluation of PD-L1, TIGIT, and CD155

The proportion of TIGIT<sup>+</sup> cytotoxic T lymphocytes was calculated as a percentage of total CD3<sup>+</sup>CD8<sup>+</sup> T lymphocytes. The proportion of CD155<sup>+</sup> and PD-L1<sup>+</sup> macrophages was calculated as a percentage of total CD68<sup>+</sup> macrophages. The proportion of TIGIT<sup>+</sup>, CD155<sup>+</sup>, and PD-L1<sup>+</sup> tumor cells (TCs) was evaluated as a percentage of the total CK<sup>+</sup> TCs. The optimal cut-off values for TIGIT, CD155, and PD-L1 expression in TCs and ICs were determined using the minimum p value approach in terms of survival outcomes. Based on the minimum p value approach, we defined 70%, 5%, and 10% as the cut-off values for cytotoxic T-lymphocyte TIGIT positivity, macrophage CD155 positivity, and macrophage PD-L1 positivity, respectively. TC TIGIT, TC CD155, and TC PD-L1 positivity rates were 10%, 50%, and 10%, respectively.

## Laser capture microdissection and RNA sequencing/whole-exome sequencing analysis

We collected five samples to perform the laser capture microdissection (LCM) and the subsequently RNA sequencing (RNA-seq)/whole-exome sequencing (WES) to elucidate potential mechanisms underlying the different immune phenotypes between SQC and ADC. Subtype-enriched regions were independently evaluated by two board-certified pathologists. Regions demonstrating  $\geq 90\%$  purity for either SQC or ADC components were selected for LCM. Tissue sections were microdissected using the Leica LMD7000 system (Leica Microsystems, Wetzlar, Germany). Genomic DNA was extracted from the dissected regions using the QIAamp DNA Micro Kit (Qiagen, Germany) in accordance with the manufacturer's protocol. Subsequently, RNA-seq and WES were performed to profile the transcriptomic and genomic landscapes of each subtype-specific region. Differentially mutated and expressed genes between SQC and ADC compartments were systematically analyzed. Gene Set Enrichment Analysis (GSEA) and pathway enrichment analyses were conducted to elucidate biological mechanisms underlying immune phenotypes. Detailed bioinformatics pipelines are described in the online supplemental methods.

## Spatial distribution recognition

Multispectral image analysis was conducted using InForm Image Analysis Software (V.2.4, PerkinElmer). Target proteins were labeled with specific antibodies conjugated to fluorophores. Single-stained slides were prepared for further analyses. A spectral library was constructed based on the emission spectra of these fluorophores, while autofluorescence spectra from tissue specimens were collected from unstained sections. This spectral library served as a reference for defining cell phenotypes, which were characterized by both the spectral properties of the fluorophores and the morphological features of the nuclei stained with 4',6-diamidino-2-phenylindole (DAPI). Using single-fluorophore spectral data, the InForm software extracted phenotypic information and applied a supervised classification approach to identify individual DAPI-stained nuclei within mixed fluorescence images.

In this study, we introduced proximity scores of infiltrated ICs as novel prognostic markers based on the colocalization of TCs and infiltrating ICs. The empirical G-cross function was computed for each sample to quantify the probability that a given TC had at least one IC within its vicinity, defined by a specific radius. This function was determined by measuring the distance from the centroid of a given IC to the nearest TC. Therefore, higher G-cross function values indicate a greater proportion of infiltrated ICs in close proximity to TCs, reflecting increased colocalization. In this study, we specifically examined the G-cross function for radii of 0–10  $\mu\text{m}$ , 0–20  $\mu\text{m}$ , and 0–30  $\mu\text{m}$ , as these distances have been previously shown to correspond to certain IC populations likely to engage in direct, effective cell-to-cell interactions with TCs.

## Statistical analyses

All statistical analyses were conducted using R software (V.4.3.3). The Mann-Whitney U test was used to compare statistical differences between continuous variables. Spearman's rank correlation coefficients were calculated to examine the correlations between two continuous variables. To determine survival and independent prognostic factors, we performed Kaplan-Meier analysis with log-rank tests, as well as univariate and multivariate Cox proportional hazards regression analyses. Variables found to be significantly associated with survival outcomes in the univariate analysis ( $p < 0.05$ ) were included in the multivariate analyses. Statistical significance was set at  $p < 0.05$ . When conducting multiple comparisons,  $p$  values were adjusted using the Benjamini-Hochberg method.

## RESULTS

### Association of immune checkpoint expression with clinicopathological features in patients with PASC

The median age of the patients in this cohort was 65 years, with 60 male patients (65.22%). 34 tumors (36.96%) were located in the pancreatic head, while 58 (63.04%) were located in the body or tail. The clinicopathological features are summarized in online supplemental table 1. Next, we evaluated the association between the density of infiltrating immune checkpoint-positive ICs and the percentage of immune checkpoint-positive TCs across distinct clinicopathological features (online supplemental figures 1–3). We found that positive expressions of PD-L1 on the macrophages (PD-L1<sup>+</sup>CD68<sup>+</sup>) and on the TCs (CK<sup>+</sup>PD-L1<sup>+</sup>) were correlated with advanced AJCC stage (PD-L1<sup>+</sup>CD68<sup>+</sup>:  $p = 0.005$ ; CK<sup>+</sup>PD-L1<sup>+</sup>:  $p = 0.008$ ), especially advanced T status (PD-L1<sup>+</sup>CD68<sup>+</sup>:  $p = 0.012$ ; CK<sup>+</sup>PD-L1<sup>+</sup>:  $p = 0.031$ ), and lower PNI incidence (PD-L1<sup>+</sup>CD68<sup>+</sup>:  $p = 0.014$ ; CK<sup>+</sup>PD-L1<sup>+</sup>:  $p = 0.018$ ; online supplemental figure 1B,C). In addition, higher expression of CD155 in macrophages (CD155<sup>+</sup>CD68<sup>+</sup>) was significantly associated with advanced AJCC status ( $p = 0.011$ ) and higher CD155 expression in TCs (CK<sup>+</sup>CD155<sup>+</sup>:  $p = 0.046$ ; online supplemental figure 1D,E). Briefly, these results indicated that higher immune checkpoint expression in ICs and TCs was related to clinically aggressive tumor phenotypes.

### Immune heterogeneity between SQC and ADC compartments in patients with PASC using a training set

To examine the distribution of infiltrating ICs within the tumor microenvironment (TME), we first used mIF to evaluate immune biomarkers and determine the spatial densities of PASCs and PDACs (table 1). A significant increase in the densities of CD3<sup>+</sup>CD8<sup>+</sup>TIGIT<sup>+</sup> cells and CD155<sup>+</sup>CD68<sup>+</sup> cells, along with a decrease in the densities of CD3<sup>+</sup> cells, consisting of CD3<sup>+</sup>CD8<sup>+</sup> and CD3<sup>+</sup>CD8<sup>+</sup>GrB<sup>+</sup> T cells, was observed within both the SQC and ADC areas of PASCs compared with PDACs in both the intraepithelial and stromal compartments. Additionally, increased densities of CD68<sup>+</sup> macrophages and PD-L1<sup>+</sup>CD68<sup>+</sup> macrophages were exclusively found in the intraepithelial

**Table 1** Analysis of immune biomarkers in the squamous cell and adenocarcinoma areas of the pancreatic adenosquamous carcinoma and the pancreatic ductal adenocarcinoma

Phenotype	PDAC		SQC components of PASC		ADC components of PASC		P value
	Median	IQR	Median	IQR	Median	IQR	
Intraepithelial compartment							
CD3 <sup>+</sup> (n/mm <sup>2</sup> )	341.64	453.96	131.44	260.77	206.16	372.93	<b>5.46E-10</b>
CD3 <sup>+</sup> CD8 <sup>+</sup> (n/mm <sup>2</sup> )	107.64	141.57	26.60	90.27	34.59	131.47	<b>3.84E-12</b>
CD3 <sup>+</sup> PD-1 <sup>+</sup> (n/mm <sup>2</sup> )	30.50	71.60	49.43	142.42	40.82	97.31	<b>0.035</b>
CD3 <sup>+</sup> CD8 <sup>+</sup> PD-1 <sup>+</sup> (n/mm <sup>2</sup> )	8.76	19.56	20.35	64.59	14.35	45.29	<b>0.004</b>
CD3 <sup>+</sup> CD8 <sup>+</sup> GrB <sup>+</sup> (n/mm <sup>2</sup> )	6.00	12.75	3.28	17.60	3.48	15.26	0.766
CD68 <sup>+</sup> (n/mm <sup>2</sup> )	139.32	129.00	577.21	621.42	722.46	956.77	<b>&lt;2.2E-16</b>
CD45RO <sup>+</sup> (n/mm <sup>2</sup> )	50.39	97.07	49.54	112.28	162.88	307.23	<b>5.00E-11</b>
Foxp3 <sup>+</sup> (n/mm <sup>2</sup> )	12.34	23.50	14.94	57.89	13.00	72.74	0.456
CD3 <sup>+</sup> CD8 <sup>+</sup> TIGIT <sup>+</sup> (%)	6.84	9.54	63.65	40.33	70.57	41.03	<b>&lt;2.2E-16</b>
CD155 <sup>+</sup> CD68 <sup>+</sup> (%)	0.94	3.66	32.37	53.69	16.03	29.78	<b>&lt;2.2E-16</b>
PD-L1 <sup>+</sup> CD68 <sup>+</sup> (%)	13.58	20.98	18.27	41.62	26.50	43.96	<b>2.47E-05</b>
Stromal compartment							
CD3 <sup>+</sup> (n/mm <sup>2</sup> )	740.22	983.58	241.77	405.92	260.47	443.05	<b>&lt;2.2E-16</b>
CD3 <sup>+</sup> CD8 <sup>+</sup> (n/mm <sup>2</sup> )	260.13	342.13	77.22	149.75	59.77	146.91	<b>&lt;2.2E-16</b>
CD3 <sup>+</sup> PD-1 <sup>+</sup> (n/mm <sup>2</sup> )	56.96	133.73	128.66	216.67	36.75	109.61	<b>3.14E-05</b>
CD3 <sup>+</sup> CD8 <sup>+</sup> PD-1 <sup>+</sup> (n/mm <sup>2</sup> )	16.90	37.75	38.26	85.99	10.40	28.98	<b>1.76E-05</b>
CD3 <sup>+</sup> CD8 <sup>+</sup> GrB <sup>+</sup> (n/mm <sup>2</sup> )	14.40	30.60	4.38	22.75	1.48	10.17	<b>2.20E-09</b>
CD68 <sup>+</sup> (n/mm <sup>2</sup> )	359.91	333.25	415.75	651.11	289.57	612.86	0.677
CD45RO <sup>+</sup> (n/mm <sup>2</sup> )	236.03	454.70	111.08	220.24	191.95	342.76	<b>5.13E-05</b>
Foxp3 <sup>+</sup> (n/mm <sup>2</sup> )	47.25	90.00	56.12	101.77	45.38	107.17	0.870
CD3 <sup>+</sup> CD8 <sup>+</sup> TIGIT <sup>+</sup> (%)	5.67	10.13	54.82	29.77	54.17	39.41	<b>&lt;2.2E-16</b>
CD155 <sup>+</sup> CD68 <sup>+</sup> (%)	1.62	6.33	6.51	17.20	4.00	8.70	<b>1.04E-07</b>
PD-L1 <sup>+</sup> CD68 <sup>+</sup> (%)	23.50	36.32	18.97	29.53	15.50	25.62	0.259
Epithelial and stromal compartment							
CD3 <sup>+</sup> (n/mm <sup>2</sup> )	569.40	756.60	242.22	332.39	263.83	364.02	<b>1.72E-14</b>
CD3 <sup>+</sup> CD8 <sup>+</sup> (n/mm <sup>2</sup> )	179.40	235.95	61.91	119.37	57.11	123.58	<b>2.71E-14</b>
CD3 <sup>+</sup> PD-1 <sup>+</sup> (n/mm <sup>2</sup> )	44.85	105.30	112.17	164.88	46.14	85.52	<b>9.72E-06</b>
CD3 <sup>+</sup> CD8 <sup>+</sup> PD-1 <sup>+</sup> (n/mm <sup>2</sup> )	15.36	34.32	34.85	75.01	12.34	28.71	<b>4.05E-05</b>
CD3 <sup>+</sup> CD8 <sup>+</sup> GrB <sup>+</sup> (n/mm <sup>2</sup> )	8.00	17.00	3.82	24.30	3.28	10.17	<b>0.004</b>
CD68 <sup>+</sup> (n/mm <sup>2</sup> )	232.20	215.00	482.53	613.55	481.57	646.90	<b>6.90E-10</b>
CD45RO <sup>+</sup> (n/mm <sup>2</sup> )	132.60	255.45	103.27	166.74	191.77	328.11	<b>0.002</b>
Foxp3 <sup>+</sup> (n/mm <sup>2</sup> )	26.25	50.00	51.04	88.57	43.84	99.52	<b>0.003</b>
CD3 <sup>+</sup> CD8 <sup>+</sup> TIGIT <sup>+</sup> (%)	4.69	8.38	55.99	30.00	60.44	40.95	<b>&lt;2.2E-16</b>
CD155 <sup>+</sup> CD68 <sup>+</sup> (%)	1.20	4.69	18.09	31.63	9.08	15.20	<b>&lt;2.2E-16</b>
PD-L1 <sup>+</sup> CD68 <sup>+</sup> (%)	17.41	26.91	19.37	31.45	24.88	28.28	<b>0.046</b>

Kruskal-Wallis test was applied. P values<0.05 are bolded.

ADC, adenocarcinoma; PASC, pancreatic adenosquamous carcinoma; PDAC, pancreatic ductal adenocarcinoma; SQC, squamous carcinoma.

compartment (figure 2), indicating different immune characteristics in the TME of PSAC compared with PDAC.

To gain deeper insights, we further analyzed ICs distribution within the SQC and ADC areas of PASC. Our analyses revealed higher densities of CD3<sup>+</sup>, CD45RO<sup>+</sup>, and

CD3<sup>+</sup>CD8<sup>+</sup>TIGIT<sup>+</sup> cells in the intraepithelial compartment of ADC areas compared with SQC areas within PASC. In contrast, CD155<sup>+</sup>CD68<sup>+</sup> cells were more abundant in the SQC areas. No significant differences were observed between SQC and ADC areas in the stromal compartment

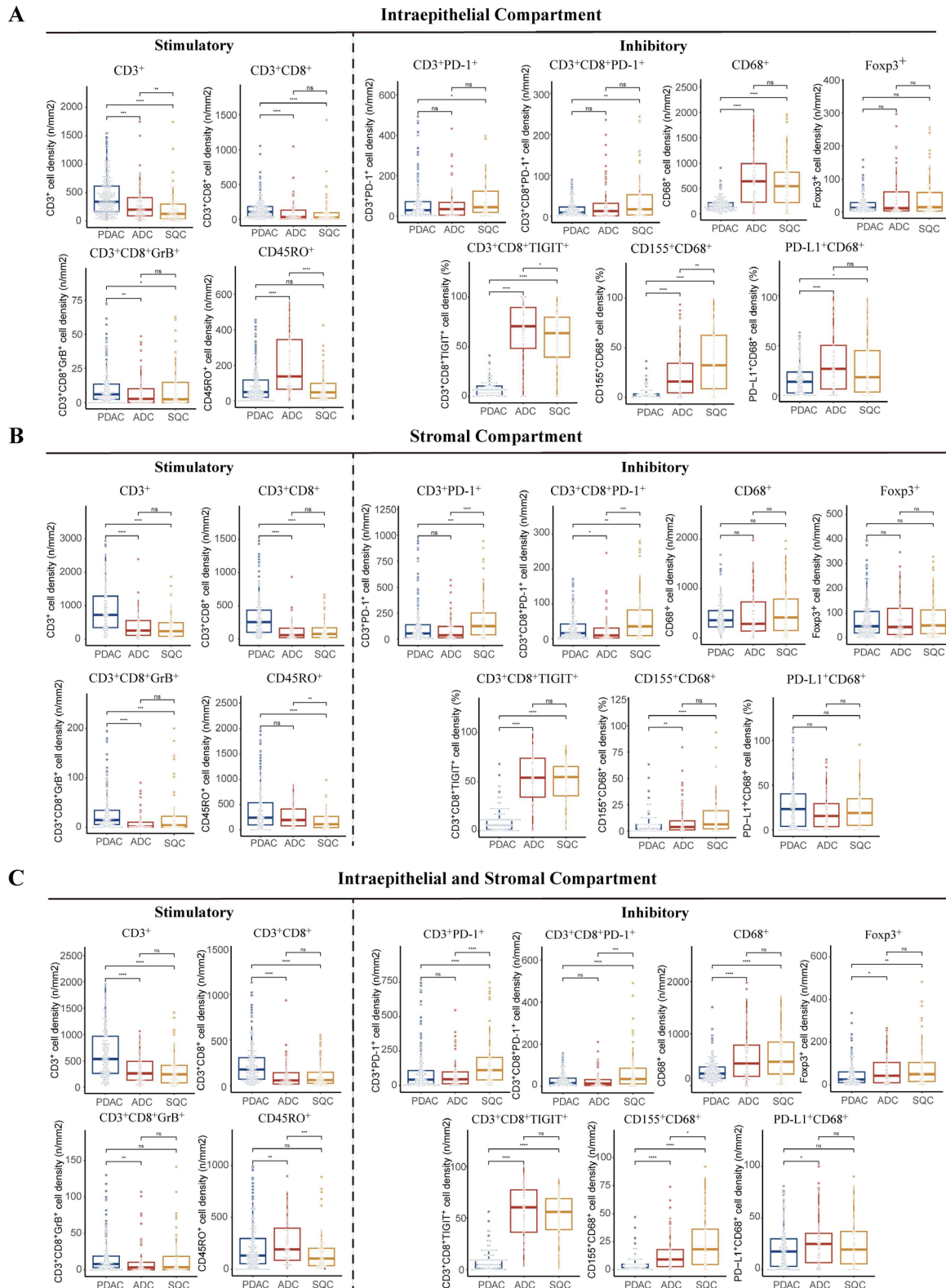


**Figure 2** Immune composition of pancreatic adenosquamous carcinoma reveals compartmentalized immunosuppressive microenvironments enriched in squamous cell (SQC) regions. (A–C) Quantitative comparison of immune cell subsets across histologic subtypes and tumor compartments. Boxplots show densities of stimulatory (CD3<sup>+</sup>, CD3<sup>+</sup>CD8<sup>+</sup>, CD3<sup>+</sup>CD8<sup>+</sup>GrB<sup>+</sup>, CD45RO<sup>+</sup>), inhibitory (CD3<sup>+</sup>PD-1<sup>+</sup>, CD3<sup>+</sup>CD8<sup>+</sup>PD-1<sup>+</sup>, CD68<sup>+</sup>, Foxp3<sup>+</sup>, CD3<sup>+</sup>CD8<sup>+</sup>TIGIT<sup>+</sup>, CD155<sup>+</sup>CD68<sup>+</sup>, PD-L1<sup>+</sup>CD68<sup>+</sup>) immune cells in: (A), the intraepithelial compartment; (B), the stromal compartment; and (C), both compartments combined. Each marker is stratified by histologic subtype: pancreatic ductal adenocarcinoma (PDAC), adenocarcinoma (ADC), and SQC compartments. Cell densities are expressed as number of positive cells per mm<sup>2</sup> or percentage of total immune cells. Differences between two groups were determined by the Mann-Whitney U test. P values were adjusted using the Benjamini-Hochberg method. \*p<0.05, \*\*p<0.01, \*\*\*p<0.001, \*\*\*\*p<0.0001; ns, not significant.

of PASC when comparing the densities of CD3<sup>+</sup>PD-1<sup>+</sup>, CD3<sup>+</sup>CD8<sup>+</sup>PD-1<sup>+</sup>, and CD45RO<sup>+</sup> cells (figure 2), highlighting the immune heterogeneity of infiltrated ICs in different pathological compartments of PASCs.

In addition, we examined the localization of infiltrating ICs within the intraepithelial and stromal regions in both SQC and ADC compartments of PASC. In the SQC compartment, CD3<sup>+</sup>-related cells (including CD3<sup>+</sup>, CD3<sup>+</sup>CD8<sup>+</sup>, CD3<sup>+</sup>PD-1<sup>+</sup>, and CD3<sup>+</sup>CD8<sup>+</sup>PD-1<sup>+</sup>), CD45RO<sup>+</sup>, and Foxp3<sup>+</sup> cells were predominantly located in the tumor stroma, while CD3<sup>+</sup>CD8<sup>+</sup>TIGIT<sup>+</sup> and CD155<sup>+</sup>CD68<sup>+</sup> cells were more prevalent in the intraepithelial regions. Moreover, in ADC areas, CD68<sup>+</sup> and PD-L1<sup>+</sup>CD68<sup>+</sup> macrophages were primarily enriched in the intraepithelial regions. Notably, the densities of CD3<sup>+</sup>CD8<sup>+</sup>TIGIT<sup>+</sup> and CD155<sup>+</sup>CD68<sup>+</sup> cells were significantly higher in the intraepithelial regions of both SQC and ADC areas than in the stromal regions (online supplemental figure 4).

Next, to assess the spatial distribution of TLS in PASC, we quantified TLS density and proximity to SQC and ADC compartments (online supplemental figure 5A). TLS were present in 45.65% (n=42) of patients, with a median count of 0.011/mm<sup>2</sup> (range, 0–0.484). The minimum distance from TLS to SQC compartments did not differ significantly from that to ADC compartments (p=0.363; online supplemental figure 5B). Moreover, correlation analysis revealed that the density of TLS was positively associated with the abundance of CD155<sup>+</sup> macrophages (p=0.019), while no significant associations were observed with other IC subsets (online supplemental figure 5C). These findings suggest a potential link between TLS presence and immunosuppressive macrophage infiltration, possibly via the TIGIT/CD155 axis.

#### Distinct expression patterns of PD-1/PD-L1 and TIGIT/CD155 reflect attenuated immune surveillance in patients with PASC

To conduct a more detailed comparison of immune checkpoint expression levels on the TCs, we identified six heterogeneous phenotypes in our panels, including TCs expressing TIGIT (CK<sup>+</sup>TIGIT<sup>+</sup>), CD155 (CK<sup>+</sup>CD155<sup>+</sup>), and PD-L1 (CK<sup>+</sup>PD-L1<sup>+</sup>; figure 3A–C), macrophages expressing PD-L1 (CD68<sup>+</sup>PD-L1<sup>+</sup>) and CD155 (CD68<sup>+</sup>CD155<sup>+</sup>), and CD8<sup>+</sup>T cells expressing TIGIT (CD8<sup>+</sup>TIGIT<sup>+</sup>). Compared with PDAC, we observed higher expression levels of CD155 and PD-L1 in TCs in PASC (figure 3B). Notably, the expression levels of CD155 in TCs (CK<sup>+</sup>CD155<sup>+</sup>) within the SQC areas of PASC was significantly higher than in the ADC areas (figure 3D).

Additionally, we evaluated the correlation between the expression levels of immune checkpoints on TCs and the density of infiltrating ICs (figure 3E,F and online supplemental figure 6). Pairwise significant correlations were observed among the expression levels of TIGIT, CD155, and PD-L1 in TCs (figure 3F). Interestingly, we found that the expression levels of PD-L1 on CD68<sup>+</sup> macrophages (PD-L1<sup>+</sup>CD68<sup>+</sup>) was significantly and positively correlated with immune checkpoint expression on TCs, and the expression levels of PD-L1 on TCs (CK<sup>+</sup>PD-L1<sup>+</sup>) were

significantly correlated with the abundance of almost all infiltrated ICs (online supplemental figure 6). These findings suggest that the expression of immune checkpoints in TCs may play a role in modulating immune phenotypes within the TME of PASC.

#### Prognostic values of the PD-L1/PD-1 and TIGIT/CD155 axes in PASC

Next, we investigated whether the expression of immune checkpoints in TCs and ICs influenced patient survival outcomes. Using the cut-off determined by the minimum p value approach, we found that higher levels of CD155 and PD-L1 in macrophages (CD155<sup>+</sup>CD68<sup>+</sup> and PD-L1<sup>+</sup>CD68<sup>+</sup>) and TIGIT in CD3<sup>+</sup>CD8<sup>+</sup> T cells (CD3<sup>+</sup>CD8<sup>+</sup>TIGIT<sup>+</sup>) were associated with worse survival outcomes in patients with PASC in terms of OS and PFS (CD3<sup>+</sup>CD8<sup>+</sup>TIGIT<sup>+</sup>: p=0.021; CD155<sup>+</sup>CD68<sup>+</sup>: p=0.018; PD-L1<sup>+</sup>CD68<sup>+</sup>: p=0.017; online supplemental figures 7 and 8). Moreover, higher expression levels of CD155 and PD-L1 in TCs were correlated with worse survival outcomes (CK<sup>+</sup>CD155<sup>+</sup>: p=0.036; CK<sup>+</sup>PD-L1<sup>+</sup>: p=0.042; online supplemental figures 7 and 8). As revealed by multivariate Cox analyses, we found that CD3<sup>+</sup>CD8<sup>+</sup>TIGIT<sup>+</sup> cells (high vs low, HR: 2.85, 95% CI (1.44 to 5.68), p=0.002), and CD155<sup>+</sup>CD68<sup>+</sup> cells (high vs low, HR: 2.15, 95% CI: 1.07 to 4.29, p=0.031) were independent prognostic biomarkers of patients with PASC in terms of OS (table 2). In summary, these findings underline the clinical significance of TIGIT/CD155 axis positivity in ICs in the survival of patients with PASC.

Furthermore, we examined the prognostic significance of IC infiltration density with respect to the intraepithelial and stromal compartments. Similar trends were observed for PD-L1<sup>+</sup>CD68<sup>+</sup> and CD155<sup>+</sup>CD68<sup>+</sup> macrophages in both compartments (intraepithelial: CD155<sup>+</sup>CD68<sup>+</sup>, p=0.049; PD-L1<sup>+</sup>CD68<sup>+</sup>, p=0.019; stromal: CD155<sup>+</sup>CD68<sup>+</sup>, p=0.022; PD-L1<sup>+</sup>CD68<sup>+</sup>, p=0.020; online supplemental figures 7 and 9). However, a higher infiltration of CD3<sup>+</sup>CD8<sup>+</sup>TIGIT<sup>+</sup> T cells was significantly associated with shorter OS within the intraepithelial regions, but not in the stromal regions (intraepithelial: OS: p=0.032; stromal: OS: p=0.380; online supplemental figure 8). Further confirmation by multivariate Cox models (table 2) indicated the varied clinical value of infiltrated ICs in defined tumor regions when predicting the survival outcomes of patients with PASC.

To elucidate the functional consequences of CD155<sup>+</sup>CD68<sup>+</sup> macrophage and TIGIT<sup>+</sup>CD8<sup>+</sup> T-cell infiltration in PASC, we performed RNA-seq analysis on five specimens stratified by the abundance of these immune populations. Tumors enriched in CD155<sup>+</sup> macrophages exhibited broad downregulation of immune effector programs, including leukocyte activation, cytotoxicity, and IC-mediated killing, indicative of a profoundly immunosuppressive microenvironment (online supplemental figure 10A,B). Conversely, tumors with high TIGIT<sup>+</sup>CD8<sup>+</sup> T-cell infiltration displayed significant enrichment of peptidase-related pathways, such as aspartic-type endopeptidase and serine hydrolase activity (online supplemental figure 10C,D), which are commonly associated with

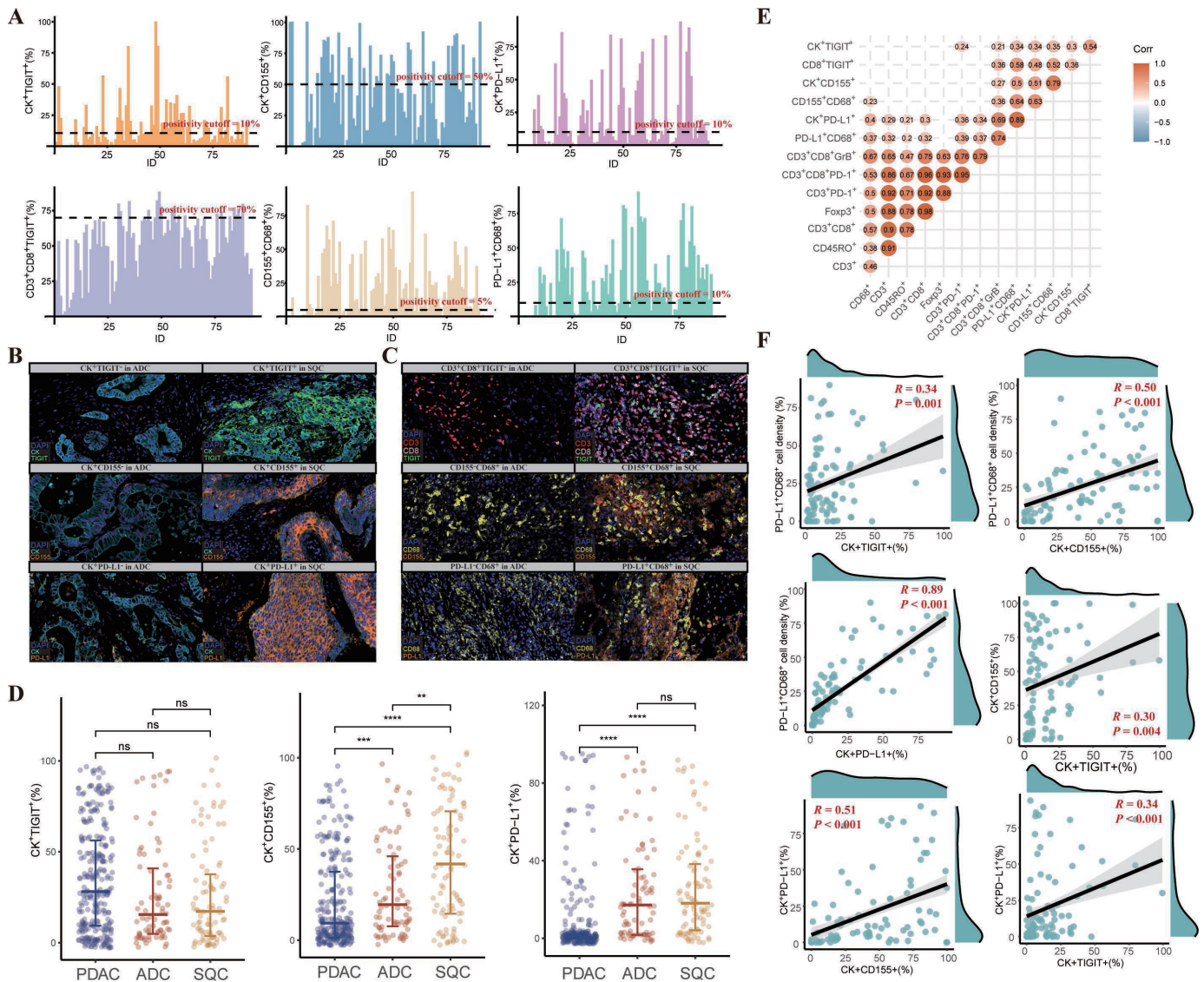


**Figure 3** Distinct immune checkpoint expression patterns in pancreatic adenosquamous carcinoma (PASC). (A) Quantification of immune checkpoint-positive cell subsets across the PASC cohort. Bar plots show the percentage of CK<sup>+</sup>TIGIT<sup>+</sup>, CK<sup>+</sup>CD155<sup>+</sup>, CK<sup>+</sup>PD-L1<sup>+</sup>, CD3<sup>+</sup>CD8<sup>+</sup>TIGIT<sup>+</sup>, CD68<sup>+</sup>CD155<sup>+</sup>, and PD-L1<sup>+</sup>CD68<sup>+</sup> cells in each patient. Positivity thresholds are indicated by dashed lines. (B–C) Representative multiplex immunofluorescence images showing spatial enrichment of immune checkpoint molecules on the tumor cells (TC; B) and immune cells (IC; C). (D) Comparison of immune checkpoint expression of the TCs across histologic subtypes. Scatter plots show the percentage of CK<sup>+</sup>TIGIT<sup>+</sup>, CK<sup>+</sup>CD155<sup>+</sup>, and CK<sup>+</sup>PD-L1<sup>+</sup> cells in PDAC, ADC, and SQC compartments. Data are presented as mean±SD. (E) Correlation matrix of immune signatures. Spearman correlation coefficients between immune cell densities and the expressions of TIGIT, CD155, and PD-L1 on the TCs and ICs were exhibited. Size and color intensity denote strength of correlation. (F) Scatter plots display significant correlations between CK<sup>+</sup>TIGIT<sup>+</sup>, CK<sup>+</sup>CD155<sup>+</sup>, CK<sup>+</sup>PD-L1<sup>+</sup>, and PD-L1<sup>+</sup>CD68<sup>+</sup> cell densities. Spearman correlation coefficients (R) and two-sided p values are shown. \*p<0.05, \*\*p<0.01, \*\*\*p<0.001, \*\*\*\*p<0.0001 and not significant (ns). Differences between two groups were determined by the Mann-Whitney U test. P values were adjusted using the Benjamini-Hochberg method. ADC, adenocarcinoma; PDAC, pancreatic ductal adenocarcinoma; SQC, squamous cell carcinoma.

extracellular matrix degradation and metastatic progression. These findings suggest that CD155<sup>+</sup> macrophages contribute to immune evasion by actively suppressing immune responses, while TIGIT<sup>+</sup>CD8<sup>+</sup> T cells may facilitate tumor invasion and dissemination through peptidase-driven remodeling of the tumor stroma. Together, these phenotypes reflect distinct, yet complementary, mechanisms of immune escape and tumor progression in PASC, offering potential targets for therapeutic intervention.

### Immune exhaustion and mutational burden define squamous compartments in PASC

To investigate the mechanisms underlying T-cell exclusion in the SQC compartments of PASC, we performed laser-capture microdissection to obtain paired SQC and ADC regions from five PASC samples exhibiting distinct abundance of T-cell infiltration between two regions. RNA-seq identified 613 differentially expressed genes, with 504 downregulated and 109 upregulated in SQC regions.

**Table 2** Univariate and multivariate analyses for the expressions of immune checkpoint on the tumor cells and immune cells in the pancreatic adenocarcinoma cohort

	No. of patients	Progression-free survival			Overall survival		
		Median survival months	Univariable HR (95% CI)	Multivariable HR (95% CI)	Median survival months	Univariable HR (95% CI)	Multivariable HR (95% CI)
Intraepithelial and stromal region							
CD3 <sup>+</sup> CD8 <sup>+</sup> TIGIT <sup>+</sup>							
<70%	71	17.3	1.00 (reference)	1.00 (reference)	27.6	1.00 (reference)	1.00 (reference)
≥70%	21	13.2	1.62 (0.94 to 2.79)	2.05 (1.09 to 3.86)	20.1	1.96 (1.10 to 3.49)	2.85 (1.44 to 5.68)
P value			0.084	0.025	<b>0.022</b>		<b>0.002</b>
CD155 <sup>+</sup> CD68 <sup>+</sup>							
<5%	25	31.5	1.00 (reference)	1.00 (reference)	38.0	1.00 (reference)	1.00 (reference)
≥5%	67	13.7	2.08 (1.15 to 3.77)	1.82 (0.98 to 3.38)	22.8	2.09 (1.12 to 3.90)	2.15 (1.07 to 4.29)
P value			<b>0.015</b>	0.060	<b>0.020</b>		<b>0.031</b>
PD-L1 <sup>+</sup> CD68 <sup>+</sup>							
<10%	31	20.8	1.00 (reference)	1.00 (reference)	36.6	1.00 (reference)	1.00 (reference)
≥10%	61	15.3	1.81 (1.06 to 3.09)	1.38 (0.78 to 2.44)	22.8	2.03 (1.13 to 3.63)	1.75 (0.91 to 3.35)
P value			<b>0.031</b>	0.270	<b>0.018</b>		0.091
CK <sup>+</sup> TIGIT <sup>+</sup>							
<10%	49	15.3	1.00 (reference)	1.00 (reference)	22.8	1.00 (reference)	1.00 (reference)
≥10%	43	27.5	0.58 (0.29 to 1.17)	1.17 (0.54 to 2.53)	34.1	0.55 (0.25 to 1.21)	1.18 (0.50 to 2.79)
P value			0.128	0.681	0.134		0.713
CK <sup>+</sup> CD155 <sup>+</sup>							
<50%	54	20.8	1.00 (reference)	1.00 (reference)	32.6	1.00 (reference)	1.00 (reference)
≥50%	38	13.1	1.69 (1.05 to 2.72)	1.23 (0.74 to 2.05)	22.8	1.72 (1.03 to 2.87)	1.40 (0.81 to 2.42)
P value			<b>0.031</b>	0.430	<b>0.037</b>		0.228
CK <sup>+</sup> PD-L1 <sup>+</sup>							
<10%	46	15.8	1.00 (reference)	1.00 (reference)	32.6	1.00 (reference)	1.00 (reference)
≥10%	46	15.8	1.58 (0.97 to 2.57)	1.42 (0.82 to 2.44)	22.8	1.71 (1.02 to 2.88)	1.69 (0.91 to 3.12)
P value			0.064	0.207	<b>0.043</b>		0.094
Intraepithelial region							
CD3 <sup>+</sup> CD8 <sup>+</sup> TIGIT <sup>+</sup>							
<70%	54	19.1	1.00 (reference)	1.00 (reference)	27.4	1.00 (reference)	1.00 (reference)
≥70%	38	13.5	1.28 (0.79 to 2.06)	1.38 (0.84 to 2.27)	22.8	1.27 (0.76 to 2.13)	1.48 (0.85 to 2.58)
P value			0.319	0.210	0.369		0.167
CD155 <sup>+</sup> CD68 <sup>+</sup>							
<10%	24	31.5	1.00 (reference)	1.00 (reference)	38.0	1.00 (reference)	1.00 (reference)
≥10%	68	13.7	1.86 (1.03 to 3.36)	1.81 (0.98 to 3.37)	22.8	1.85 (0.99 to 3.44)	2.17 (1.08 to 4.35)
P value			<b>0.040</b>	0.060	0.053		0.029
PD-L1 <sup>+</sup> CD68 <sup>+</sup>							
<5%	26	31.4	1.00 (reference)	1.00 (reference)	38.0	1.00 (reference)	1.00 (reference)
≥5%	66	15.3	1.85 (1.05 to 3.27)	1.42 (0.77 to 2.60)	22.8	2.06 (1.12 to 3.80)	1.92 (0.97 to 3.79)
P value			<b>0.035</b>	0.257	<b>0.021</b>		0.060
Stromal region							
CD3 <sup>+</sup> CD8 <sup>+</sup> TIGIT <sup>+</sup>							
<20%	13	20.8	1.00 (reference)	1.00 (reference)	49.3	1.00 (reference)	1.00 (reference)
≥20%	79	15.3	2.29 (1.04 to 5.05)	1.75 (0.73 to 4.20)	22.8	2.37 (1.06 to 5.29)	2.54 (1.00 to 6.46)
P value			<b>0.040</b>	0.214	<b>0.036</b>		<b>0.050</b>

Continued

**Table 2** Continued

	No. of patients	Progression-free survival			Overall survival		
		Median survival months	Univariable HR (95% CI)	Multivariable HR (95% CI)	Median survival months	Univariable HR (95% CI)	Multivariable HR (95% CI)
<b>CD155<sup>+</sup>CD68<sup>+</sup></b>							
<1%	19	20.8	1.00 (reference)	1.00 (reference)	38.0	1.00 (reference)	1.00 (reference)
≥1%	73	15.3	1.67 (0.89 to 3.14)	1.41 (0.71 to 2.77)	22.8	2.32 (1.13 to 4.77)	2.49 (1.11 to 5.57)
P value			0.111	0.324		<b>0.022</b>	<b>0.027</b>
<b>PD-L1<sup>+</sup>CD68<sup>+</sup></b>							
<10%	33	20.8	1.00 (reference)	1.00 (reference)	36.6	1.00 (reference)	1.00 (reference)
≥10%	59	15.3	1.93 (1.13 to 3.29)	1.55 (0.88 to 2.74)	22.8	1.97 (1.11 to 3.49)	1.77 (0.95 to 3.31)
P value			<b>0.016</b>	0.129		<b>0.020</b>	0.072

The multivariable Cox regression model initially included sex, age, tumor size, tumor location, serum CA19-9 levels, AJCC, LVI and PNI. P values <0.05 are bolded. AJCC, American Joint Committee on Cancer; CA19-9, carbohydrate antigen 19-9; LVI, lymphovascular invasion; PNI, perineural invasion.

Consistent with previous findings, GSEA revealed down-regulation of pathways related to immune response regulation (False Discovery Rate [FDR]= $7.31 \times 10^{-13}$ ) and T-cell differentiation (FDR= $2.0 \times 10^{-5}$ ) in SQC regions (online supplemental figure 11A). Notably, multiple immune exhaustion markers, including *PDCD1* (p=0.009), *CTLA4* (p=0.021), *LAG3* (p=0.010), *HAVCR2* (p=0.006), and *TIGIT1* (p=0.001), were significantly upregulated in the SQC regions compared with ADC regions (online supplemental figure 11B), consistent with an exhausted immune phenotype.

Antigen processing and presentation pathways via major histocompatibility complex class I (FDR=0.967) and class II (FDR=0.526) showed no significant differences between compartments (online supplemental figure 11C). However, differential expression of key antigen-processing molecules was observed in SQC areas, including upregulation of *B2M* (p=0.045) and *ERAP2* (p=0.036), and downregulation of *CALR* (p=0.037; online supplemental figure 11D), suggesting altered antigen presentation may contribute to immune modulation.

Somatic mutation analysis revealed recurrent alterations in *MAP2K3*, *NOD2*, and *INHBC* in SQC regions (online supplemental figure 12A), implicating these genes as potential tumor-associated antigens (TAA), enriched in MAPK signaling and efferocytosis pathways (online supplemental figure 12B). Notably, tumor mutational burden was significantly higher in SQC compared with ADC regions (p=0.0098; online supplemental figure 12C), providing a rationale for TAA-based immunotherapeutic strategies.

### Compartment-specific spatial organization of tumor and immune cells in PASC

Given our ability to precisely define the positions of individual TCs and ICs, we examined the spatial organization of these cells and their clinical significance in PASC. To

further quantify the localization patterns, we introduced G-cross-function values, which represent the probability of detecting at least one given infiltrated ICs within a given radius of any TCs (figure 4A). Hence, a higher G-cross-function value indicates a higher density of infiltrated ICs surrounding the TCs within a specific distance. As shown in figure 4B and online supplemental figure 13, compared with PDAC, PASC exhibited higher G-cross function values for CD45RO<sup>+</sup> cells and PD-1<sup>+</sup>CD3<sup>+</sup>CD8<sup>+</sup> cells but lower values for CD3<sup>+</sup>CD8<sup>+</sup>GrB<sup>+</sup> cells across all the three considered distances (0–10/0–20/0–30 μm). Interestingly, we also found that CD45RO<sup>+</sup> cells and CD3<sup>+</sup>CD8<sup>+</sup>GrB<sup>+</sup> cells had significantly higher G-cross-function values in ADC areas of the PASC within all three distances compared with SQC areas (figure 4B and online supplemental figure 13). Next, we assessed the spatial distribution of infiltrating ICs and the expression of immune checkpoints among different PC subtypes. Across all distances considered, PASC showed significantly higher G-cross-function values for TIGIT<sup>+</sup>CD3<sup>+</sup>CD8<sup>+</sup> PASC compared with PDAC (figure 4C). Moreover, compared with the ADC areas of PASC, higher G-cross function values of CD155<sup>+</sup>CD68<sup>+</sup> cells and PD-L1<sup>+</sup>CD68<sup>+</sup> cells were observed in the SQC areas (figure 4C), highlighting the spatial heterogeneity of IC infiltration within different compartments of PASC.

Furthermore, we determined whether the spatial organization of ICs within PASC was correlated with patient survival outcomes. We found that patients with PASC and higher G-cross function values of CD68<sup>+</sup> cells and CD155<sup>+</sup>CD68<sup>+</sup> cells (radius of 0–10 μm) in ADC areas (CD68<sup>+</sup>(0–10 μm): p=0.037; CD68<sup>+</sup>(0–20 μm): p=0.024; CD68<sup>+</sup>(0–30 μm): p=0.024; CD155<sup>+</sup>CD68<sup>+</sup>(0–10 μm): p=0.025) exhibited significantly shorter OS, and G-cross function values of Foxp3<sup>+</sup> cells (radius of 0–10 μm) and CD3<sup>+</sup>CD8<sup>+</sup>GrB<sup>+</sup> cells (radius of 0–20 μm) in SQC areas

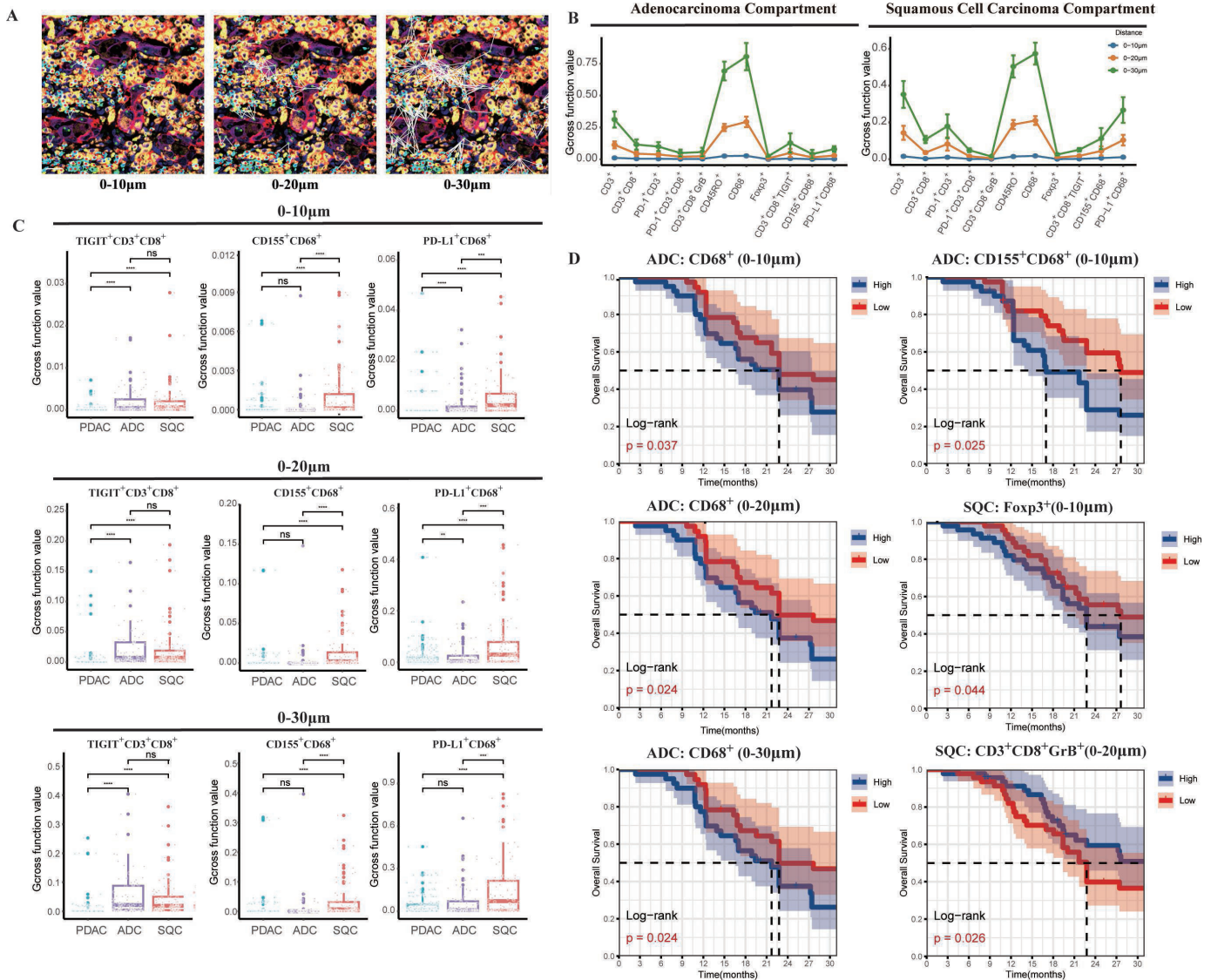


**Figure 4** Spatial profiling of immunosuppressive phenotypes and their prognostic relevance in pancreatic adenocarcinomas (PASC). (A) Illustration of the distance analysis involving immune and tumor cells. Red dots: tumor cells; green dots: immune cells. Scale bar: 200  $\mu\text{m}$ . (B) Distance-dependent enrichment of immune cell (IC) phenotypes. Line plots of mean G-cross function values for each immune marker pair in adenocarcinoma (ADC) and squamous carcinoma (SQC) regions across three distance bins (0–10/0–20/0–30  $\mu\text{m}$ ). Squamous compartments showed greater proximity-based enrichment of suppressive phenotypes. (C) Quantitative comparison of immune checkpoint-positive ICs across tumor compartments. Boxplots show G-cross function values of TIGIT<sup>+</sup>CD3<sup>+</sup>CD8<sup>+</sup> T cells, CD155<sup>+</sup>CD68<sup>+</sup> macrophages, and PD-L1<sup>+</sup>CD68<sup>+</sup> macrophages in PDAC, ADC, and SQC samples across increasing tumor-edge distances (0–10/0–20/0–30  $\mu\text{m}$ ). Squamous compartments consistently exhibited higher suppressive colocalization. (D) Prognostic relevance of spatially localized ICs in patients with PASC based on the effective densities (0–10/0–20/0–30  $\mu\text{m}$ ). The individual immune infiltrate values were divided into high ( $\geq$ half of the patients in the cohort; blue line) or low density ( $<$ half of patients in the cohort; red line). \* $p < 0.05$ , \*\* $p < 0.01$ , \*\*\* $p < 0.001$ , \*\*\*\* $p < 0.0001$  and not significant (ns). Differences between two groups were determined by the Mann-Whitney U test. Log-rank p values are indicated in the Kaplan-Meier survival analysis. P values were adjusted using the Benjamini-Hochberg method. PDAC, pancreatic ductal adenocarcinoma.

also demonstrated significantly association with OS (Foxp3<sup>+</sup>(0–10  $\mu\text{m}$ ):  $p = 0.044$ ; CD3<sup>+</sup>CD8<sup>+</sup>GrB<sup>+</sup> (0–20  $\mu\text{m}$ ):  $p = 0.026$ ; figure 4D and online supplemental figures 14–16). However, after considering the significant clinicopathological features in the multivariate Cox models, no IC phenotype showed correlation with OS (online supplemental tables 7 and 8). These findings indicate that the comprehensive abundance of infiltrating IC, rather than

the detailed spatial organization, plays a more important role in prognosis prediction in patients with PASC.

#### Validation of immune profiles and spatial organization in PASC using a validation set

To validate these findings, we analyzed an independent cohort of 28 surgically resected PASC specimens (online supplemental table 2). Consistent with our primary

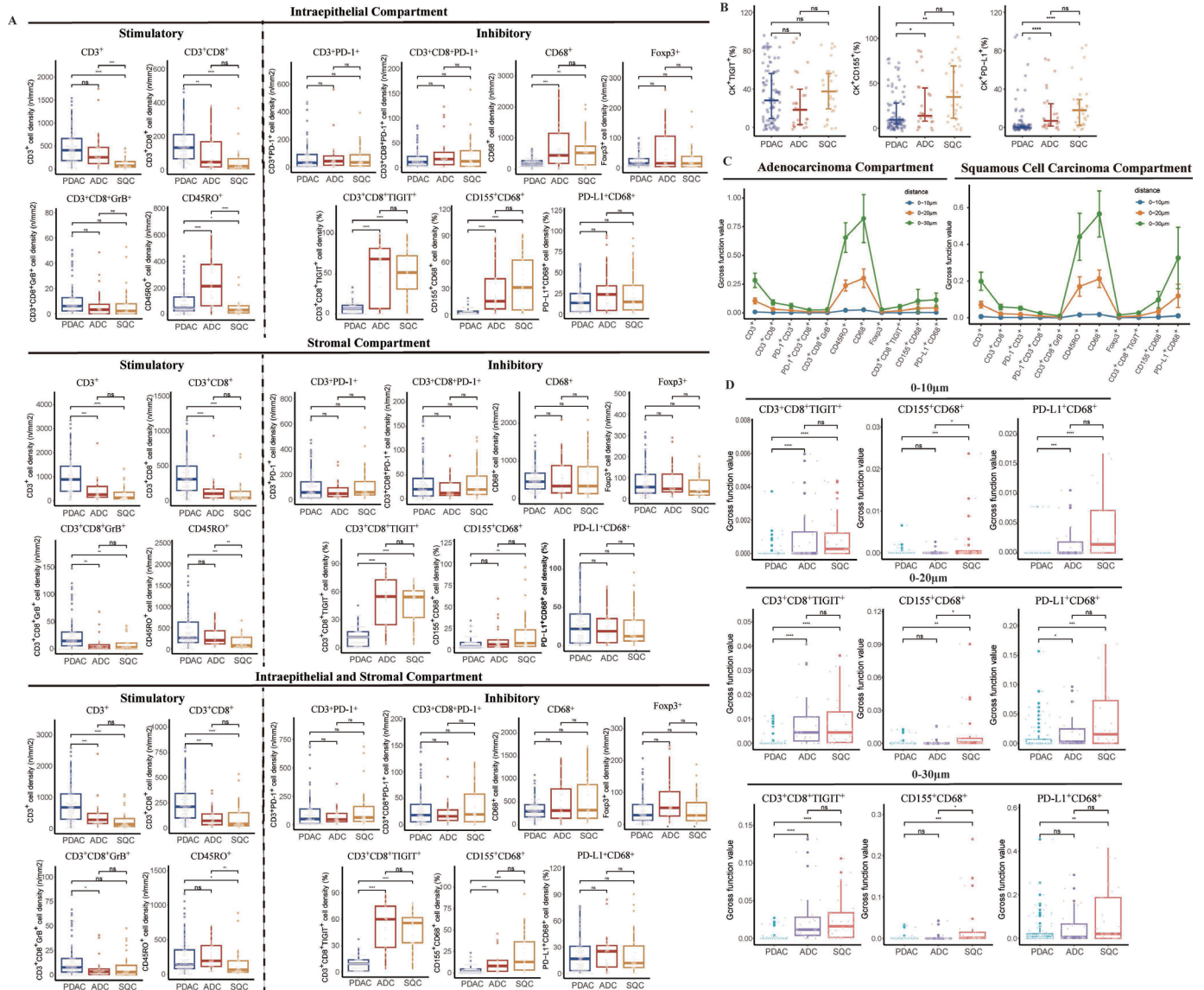


**Figure 5** Validation of immune composition and spatial immunosuppressive signatures in pancreatic adenosquamous carcinomas (PASC). (A) Immune cell (IC) infiltration and phenotypic composition across tumor compartments. Boxplot displaying differential distribution of immune cell densities, characterized by stimulatory or inhibitory markers, among the intraepithelial (upper), stromal (middle), and total (lower) compartments of the validation PASC cohort, among areas of squamous cell (SQC), and adenocarcinoma (ADC) compartment, and the validation pancreatic ductal adenocarcinoma (PDAC) cohort. (B) Scatter dot plot showing the different expression patterns of immune checkpoint on tumor cells among the SQC, ADC compartments of the validation PASC cohort, and the validation PDAC cohort. (C) The distance-based distribution of the IC abundance, measured by G-cross function values, in the tumor core within 10, 20 and 30  $\mu\text{m}$  increments in the SQC and ADC compartments of PASC in the validation PASC cohort. (D) Spatial proximity exhibits immunosuppressive cell interactions in SQC regions. Boxplot presenting distributions of immune checkpoint expression on the ICs among SQC and ADC compartments of the PASC, and PDAC in the tumor core within 10, 20 and 30  $\mu\text{m}$  increments in the validation cohorts. \* $p < 0.05$ , \*\* $p < 0.01$ , \*\*\* $p < 0.001$ , \*\*\*\* $p < 0.0001$  and not significant (ns). Differences between two groups were determined by the Mann-Whitney U test. P values were adjusted using the Benjamini-Hochberg method.

cohort, PASCs exhibited significantly lower densities of  $\text{CD3}^+$  and  $\text{CD3}^+\text{CD8}^+$  cells in both epithelial and stromal compartments compared with PDACs, regardless of SQC or ADC regions. Additionally, we observed increased  $\text{CD68}^+$  macrophages densities in the intraepithelial compartment and decreased densities of  $\text{CD3}^+\text{CD8}^+\text{GrB}^+$  cells in the stromal compartment (figure 5A). Within PASC, ADC areas exhibited higher densities of  $\text{CD3}^+$  and  $\text{CD45RO}^+$  cells in the intraepithelial compartment

compared with the SQC areas. Moreover, consistent with previous findings, high expression of TIGIT on  $\text{CD8}^+$  T cells ( $\text{CD3}^+\text{CD8}^+\text{TIGIT}^+$ ) and CD155 on macrophages ( $\text{CD155}^+\text{CD68}^+$ ) was observed in PASCs compared with PDACs, regardless of ADC and SQC regions (figure 5B). It was also confirmed that higher expressions of CD155 and PD-L1 on TCs ( $\text{CK}^+\text{CD155}^+$  and  $\text{CK}^+\text{PD-L1}^+$ ) was observed in PASC, while no difference was observed between the ADC and SQC regions (figure 5B).

Furthermore, the spatial organization of infiltrating ICs in the validation cohort aligned with our previous findings. Compared with PDACs, PASCs exhibited higher G-cross-function values for CD45RO<sup>+</sup> cells across all three analyzed distances, with ADC areas showing particularly elevated values (figure 5C and online supplemental figures 17). Additionally, we validated for infiltrated immune checkpoint-positive ICs, and observed that higher infiltrated CD3<sup>+</sup>CD8<sup>+</sup>TIGIT<sup>+</sup> and PD-L1<sup>+</sup>CD68<sup>+</sup> cells were displayed in PASCs across all three considered distances, compared with PDACs, and richer infiltration of CD155<sup>+</sup>CD68<sup>+</sup> cells was observed in the SQC areas of PASCs (figure 5D). These results, based on the validation cohort, further demonstrated the unique infiltration patterns and immune phenotypes of PASC.

## DISCUSSION

PASC is a rare but highly aggressive subtype of PC, and its immune landscape has not been previously investigated. In this study, we systematically profiled the TIME of PASC and compared IC infiltration patterns among PDAC, SQC, and ADC compartments using mIHC combined with image analysis, providing insights into the tumor heterogeneity of PASC. Furthermore, we comprehensively analyzed the complex IC phenotypes and characterized the expression landscape of immune checkpoint molecules, including the PD-1/PD-L1 and TIGIT/CD155 axes, in PASC, assessing their clinical significance in relation to patient survival outcomes.

The TIME, which contains multiple low-immunogenic components, plays a pivotal role in the progression and immune evasion of PCs. A comparative study of the TIME of PASC and PDAC was derived from a previous clinical observation that patients with PASC exhibited inferior survival outcomes. Our findings revealed that, compared with PDAC, the overall TIME of PASC exhibited immunosuppression, characterized by a significantly decreased abundance of T cells, particularly effector T cells, such as cytotoxic T lymphocytes and activated cytotoxic T lymphocytes. Interestingly, although a previous study indicated that the genetic landscape of these subtypes shares similar features,<sup>8</sup> intrinsic immune heterogeneity was observed between the SQC and ADC compartments of PASC. We found that distinct IC patterns were characterized by an elevated abundance of antigen-experienced T lymphocytes, including antigen-experienced cytotoxic T lymphocytes, in the SQC compartment of PASC, particularly in the stromal area. These conclusions highlight that the immunosuppressive TME may contribute to a poorer prognosis in patients with PASC than in those with PDAC. Moreover, the immune heterogeneity between the SQC and ADC components within PASC underscores the need for further investigation into tumor biology and the development of targeted therapeutic strategies.

Owing to the poor response rate, immunotherapy targeting immune checkpoint molecules has not been recommended for most patients with PCs in clinical

practice guidelines.<sup>19–21</sup> Therefore, for patients with PASC, a progressive subtype of PCs, it is crucial to identify more accurate biomarkers to guide precision treatment. In our study, the aberrant expression patterns of immune checkpoint molecules, including the PD-1/PD-L1 and TIGIT/CD155 axes, on ICs and TCs were identified as prognostic biomarkers in patients with PASC. Among our 92 archived PASC specimens, higher expression levels of PD-L1 and CD155 in both macrophages and TCs were significantly associated with advanced AJCC staging. In addition, the overall densities of TIGIT<sup>+</sup>CD8<sup>+</sup> T cells and CD155<sup>+</sup> macrophages were associated with poorer survival outcomes and served as independent indicators, with stromal densities contributing significantly. These findings are consistent with previous studies on other malignancies. For instance, Tang *et al* demonstrated that an elevated abundance of TIGIT<sup>+</sup>CD8<sup>+</sup> T cells was associated with poorer survival outcomes by downregulation of T cells response and decreased expression of tumor necrosis factor- $\alpha$  (TNF- $\alpha$ ), interferon- $\gamma$  (IFN- $\gamma$ ), and T cell factor-1 (TCF-1) in extrahepatic cholangiocarcinoma.<sup>22</sup> A correlation between prognosis and CD155 positivity in macrophages has also been observed in breast cancer.<sup>23</sup> Notably, the abundance of infiltrating CD3<sup>+</sup>CD8<sup>+</sup>GrB<sup>+</sup> T cells was positively associated with all immune checkpoint molecules in TCs, suggesting an immunoreactive effect modulated by the expression of both axes. Our findings support the prognostic significance of the spatial perturbation of immune checkpoint expression in PASC.

Compared with PDAC, PASC is associated with significantly worse postoperative outcomes, with median OS ranging from 4.4 to 13.1 months.<sup>3,24</sup> Despite this aggressive clinical course, there are currently no prospective studies specifically evaluating the efficacy of immunotherapy in PASC, and patients are typically managed with PDAC-based chemotherapy regimens, which offer limited benefit.<sup>25</sup> In our study, we identified elevated expression of immune checkpoints PD-L1 and CD155 in PASC relative to PDAC, suggesting that immune checkpoint inhibitors (ICIs), such as pembrolizumab, may represent a rational therapeutic strategy. Notably, previous case reports have documented favorable responses to ICI in some patients with PASC,<sup>26,27</sup> and our analysis across two independent cohorts provides broader evidence supporting the potential utility of immunotherapy in this setting.

However, spatial profiling of the TME revealed significantly reduced T-cell infiltration in the SQC compared with the ADC components of PASC, reinforcing the immunologically “cold” phenotype of SQC regions. This may limit the efficacy of ICIs in isolation. Prior studies have demonstrated that certain chemotherapeutic agents, such as PT-112, crizotinib, and gemcitabine, can enhance T-cell recruitment and promote immunogenic remodeling of the TME.<sup>28–30</sup> These findings suggest that rational combinations of ICIs with immunomodulatory chemotherapy may potentiate antitumor immune responses and improve clinical outcomes in patients with

PASC. Prospective trials are warranted to evaluate these strategies in this therapeutically underserved population.

To take a step further, although the combinatorial treatment of immunotherapy targeting PD-1/PD-L1 and TIGIT/CD155 axes has not been investigated in patients with PASC, its clinical benefits have been demonstrated in multiple solid tumors. For instance, the combination of tiragolumab, atezolizumab, and bevacizumab showed satisfactory efficacy in unresectable hepatocellular carcinoma, with an ORR of 43%, above the combination of atezolizumab and bevacizumab (ORR 11%) in stage Ib-II clinical trials.<sup>31</sup> For the first time, we observed a higher expression level of CD155 and PD-L1 in both ICs and TCs in PASC than in PDAC. Interestingly, higher expression of CD155 was observed in the SQC compartment of PASC, compared with the ADC compartment. These results highlighted the potential of combinatorial immunotherapy targeting CD155 and PD-L1 in patients with PASC.

In addition to the abundance of infiltrating ICs, the density and spatial patterns of ICs account for the heterogeneity of the TIME and are associated with the prognosis of PASC. In our study, to further explore the underlying biological mechanisms, we applied the G-cross algorithm to quantify the immune-tumor distances with three distances (0–10/0–20/0–30  $\mu\text{m}$ ), which were selected based on biologically relevant ranges for antigen recognition, presentation, and immune synapse formation, as established in prior literature.<sup>32–33</sup> Using G-cross scores, we observed a decreased spatial density of activated cytotoxic T lymphocytes ( $\text{CD}3^+\text{CD}8^+\text{GrB}^+$ ) cells in the SQC compartments across all three distances. Granzyme B-mediated cytotoxicity is a key effector mechanism of  $\text{CD}8^+$  T cells, and its efficacy is highly dependent on close cell-cell proximity. Specifically, the release of granzyme B into the immunological synapse requires tight interaction between  $\text{CD}8^+$  T cells and their target cells to ensure its intracellular delivery and apoptotic induction in TCs.<sup>34</sup> Our findings thus support a spatially restricted and functionally impaired cytotoxic T-cell response in the SQC compartment, consistent with an immunosuppressive phenotype relative to the ADC regions. Furthermore, we detected increased proximal densities of  $\text{CD}155^+$  and  $\text{PD-L1}^+$  macrophages in the SQC regions across all distances examined. Prior studies have demonstrated that elevated expression of PD-L1 and CD155 on macrophages is associated with M2-like polarization, characterized by upregulation of M2-related gene signatures and immunosuppressive chemokines.<sup>35–37</sup> Notably, a previous study has reported that exosomes carrying secreted PD-L1 derived from TCs have also been implicated in promoting M2 macrophage polarization and expanding  $\text{PD-L1}^+$  macrophage populations in melanoma.<sup>38</sup> These findings underscore the biological relevance of our spatial proximity-based analyses, particularly in the context of the immunosuppressive tumor microenvironment.

Furthermore, we found that, compared with PDAC, a higher G-cross density of  $\text{TIGIT}^+\text{CD}3^+\text{CD}8^+$  cells was exhibited in PASC, and richer  $\text{CD}155^+$  and  $\text{PD-L1}^+$  macrophages

were observed in the SQC compartment of PASC. These findings indicate that immune escape based on immune checkpoint modulation may be the core reason for the immunosuppressive TME in patients with PASC, further supporting the potential of combinatorial immunotherapy targeting immune checkpoints, particularly the TIGIT/CD155 and PD-1/PD-L1 axes, in patients with PASC.

This study had some limitations. First, both the training and validation cohorts were recruited from a single institution, which may limit the generalizability of the conclusions. However, as a tier one hospital in PCs, our patients were nationwide, increasing the representativeness of the cohort. Moreover, despite the multiple advantages of mIHC method over traditional IHC, a standardized panel of protein markers for myeloid-derived suppressor cells has yet to be established. Therefore, differences in marker selection are likely to occur across studies. To address this limitation, future research should incorporate spatial transcriptomics along with comprehensive *in vivo* validation, which could offer valuable biological insights into the role of infiltrating ICs and their spatial organization in PASC.

In conclusion, PASC harbors an immunosuppressive TME and exhibits unique expression patterns of immune checkpoint molecules. Distinct TIME characteristics were identified between the SQC and ADC compartments of PASC, highlighting the complexity and heterogeneity of the immune profiles. In addition, we highlighted the prognostic significance of immune checkpoint molecules, in both TCs and ICs, providing a promising target for the treatment of PASC that warrants further investigation in clinical practice.

X Xinyuan Chen @chen\_xinyu7185

**Acknowledgements** We thank all the patients who donate their specimens in this study and colleagues from Peking Union Medical College Hospital who participated in this study.

**Contributors** XiaC, XinC and JC designed the study design. XinC, SS, SL and XiaC performed the methodology and interpretation of data. XinC, XiaC and SY contributed to the acquisition of specimens. XinC and XiaC drafted the original manuscript draft. XinC, SS, SL, SY, XiaC and JC revised and approved the final version of the manuscript. XiaC is the guarantor of the manuscript.

**Funding** This study was supported by the grants from Beijing Natural Science Foundation (No.7254398) and National Scientific Data Sharing Platform for Population and Health (NCMI-YF01N-201906).

**Competing interests** None declared.

**Patient consent for publication** Not applicable.

**Ethics approval** This study involves human participants and was approved by the Institutional Review Board of PUMCH (S-K1593) and Shandong Provincial Hospital (No. 2022–178). Written informed consent was obtained from all participants.

**Provenance and peer review** Not commissioned; externally peer reviewed.

**Data availability statement** Data are available upon reasonable request. All data generated and the code used and/or analyzed during the current study are available from the corresponding author on reasonable request.

**Supplemental material** This content has been supplied by the author(s). It has not been vetted by BMJ Publishing Group Limited (BMJ) and may not have been peer-reviewed. Any opinions or recommendations discussed are solely those of the author(s) and are not endorsed by BMJ. BMJ disclaims all liability and responsibility arising from any reliance placed on the content. Where the content includes any translated material, BMJ does not warrant the accuracy and reliability

of the translations (including but not limited to local regulations, clinical guidelines, terminology, drug names and drug dosages), and is not responsible for any error and/or omissions arising from translation and adaptation or otherwise.

**Open access** This is an open access article distributed in accordance with the Creative Commons Attribution Non Commercial (CC BY-NC 4.0) license, which permits others to distribute, remix, adapt, build upon this work non-commercially, and license their derivative works on different terms, provided the original work is properly cited, appropriate credit is given, any changes made indicated, and the use is non-commercial. See <http://creativecommons.org/licenses/by-nc/4.0/>.

#### ORCID iDs

Xinyuan Chen <http://orcid.org/0009-0007-9191-2521>

Shuofeng Li <http://orcid.org/0000-0003-2747-9501>

Jie Chen <http://orcid.org/0000-0002-2658-9525>

#### REFERENCES

- Siegel RL, Miller KD, Wagle NS, *et al*. Cancer statistics, 2023. *CA Cancer J Clin* 2023;73:17–48.
- Hester CA, Augustine MM, Choti MA, *et al*. Comparative outcomes of adenocarcinoma of the pancreas: An analysis of the National Cancer Database. *J Surg Oncol* 2018;118:21–30.
- Boyd CA, Benarroch-Gampel J, Sheffield KM, *et al*. 415 patients with adenocarcinoma of the pancreas: a population-based analysis of prognosis and survival. *J Surg Res* 2012;174:12–9.
- Regi P, Butturini G, Malleo G, *et al*. Clinicopathological features of adenocarcinoma of the pancreas. *Langenbecks Arch Surg* 2011;396:217–22.
- Imaoka H, Shimizu Y, Mizuno N, *et al*. Clinical characteristics of adenocarcinoma of the pancreas: a matched case-control study. *Pancreas* 2014;43:287–90.
- Liu C, Karam R, Zhou Y, *et al*. The UPF1 RNA surveillance gene is commonly mutated in pancreatic adenocarcinoma. *Nat Med* 2014;20:596–8.
- Brody JR, Costantino CL, Potoczek M, *et al*. Adenocarcinoma of the pancreas harbors KRAS2, DPC4 and TP53 molecular alterations similar to pancreatic ductal adenocarcinoma. *Mod Pathol* 2009;22:651–9.
- Fang Y, Su Z, Xie J, *et al*. Genomic signatures of pancreatic adenocarcinoma (PASC). *J Pathol* 2017;243:155–9.
- Kabacaoglu D, Ciecieski KJ, Ruess DA, *et al*. Immune Checkpoint Inhibition for Pancreatic Ductal Adenocarcinoma: Current Limitations and Future Options. *Front Immunol* 2018;9:1878.
- Bear AS, Vonderheide RH, O'Hara MH. Challenges and Opportunities for Pancreatic Cancer Immunotherapy. *Cancer Cell* 2020;38:788–802.
- Ho WJ, Jaffee EM, Zheng L. The tumour microenvironment in pancreatic cancer - clinical challenges and opportunities. *Nat Rev Clin Oncol* 2020;17:527–40.
- Zhao X, Li H, Lyu S, *et al*. Single-cell transcriptomics reveals heterogeneous progression and EGFR activation in pancreatic adenocarcinoma. *Int J Biol Sci* 2021;17:2590–605.
- Yu X, Harden K, Gonzalez LC, *et al*. The surface protein TIGIT suppresses T cell activation by promoting the generation of mature immunoregulatory dendritic cells. *Nat Immunol* 2009;10:48–57.
- Heiduk M, Klimova A, Reiche C, *et al*. TIGIT Expression Delineates T-cell Populations with Distinct Functional and Prognostic Impact in Pancreatic Cancer. *Clin Cancer Res* 2023;29:2638–50.
- Freed-Pastor WA, Lambert LJ, Ely ZA, *et al*. The CD155/TIGIT axis promotes and maintains immune evasion in neoantigen-expressing pancreatic cancer. *Cancer Cell* 2021;39:1342–60.
- Li M, Xia P, Du Y, *et al*. T-cell immunoglobulin and ITIM domain (TIGIT) receptor/poliiovirus receptor (PVR) ligand engagement suppresses interferon- $\gamma$  production of natural killer cells via  $\beta$ -arrestin 2-mediated negative signaling. *J Biol Chem* 2014;289:17647–57.
- Ma H, Chen X, Mo S, *et al*. The spatial coexistence of TIGIT/CD155 defines poorer survival and resistance to adjuvant chemotherapy in pancreatic ductal adenocarcinoma. *Theranostics* 2023;13:4601–14.
- Cho BC, Abreu DR, Hussein M, *et al*. Tiragolumab plus atezolizumab versus placebo plus atezolizumab as a first-line treatment for PD-L1-selected non-small-cell lung cancer (CITYSCAPE): primary and follow-up analyses of a randomised, double-blind, phase 2 study. *Lancet Oncol* 2022;23:781–92.
- Patnaik A, Kang SP, Rasco D, *et al*. Phase I Study of Pembrolizumab (MK-3475; Anti-PD-1 Monoclonal Antibody) in Patients with Advanced Solid Tumors. *Clin Cancer Res* 2015;21:4286–93.
- O'Reilly EM, Oh D-Y, Dhani N, *et al*. Durvalumab With or Without Tremelimumab for Patients With Metastatic Pancreatic Ductal Adenocarcinoma: A Phase 2 Randomized Clinical Trial. *JAMA Oncol* 2019;5:1431–8.
- Principe DR, Korc M, Kamath SD, *et al*. Trials and tribulations of pancreatic cancer immunotherapy. *Cancer Lett* 2021;504:1–14.
- Tang T, Wang W, Gan L, *et al*. TIGIT expression in extrahepatic cholangiocarcinoma and its impact on CD8+ T cell exhaustion: implications for immunotherapy. *Cell Death Dis* 2025;16:90.
- Yong H, Cheng R, Li X, *et al*. CD155 expression and its prognostic value in postoperative patients with breast cancer. *Biomed Pharmacother* 2019;115:108884.
- Katz MHG, Taylor TH, Al-Refaie WB, *et al*. Adenosquamous versus adenocarcinoma of the pancreas: a population-based outcomes analysis. *J Gastrointest Surg* 2011;15:165–74.
- Borazanci E, Millis SZ, Korn R, *et al*. Adenosquamous carcinoma of the pancreas: Molecular characterization of 23 patients along with a literature review. *World J Gastrointest Oncol* 2015;7:132–40.
- Ahmed M, Larson BK, Osipov A, *et al*. A case of adenocarcinoma pancreatic cancer with a KRAS G12C mutation with an exceptional response to immunotherapy. *Oncotarget* 2024;15:741–7.
- Liu Q, Li R, Zhu W, *et al*. Case report: Microsatellite instability-high pancreas adenocarcinoma with postoperative liver metastasis recurrence treated with multimodality therapy achieving complete pathological response. *Front Immunol* 2024;15:1456343.
- Yamazaki T, Buqué A, Ames TD, *et al*. PT-112 induces immunogenic cell death and synergizes with immune checkpoint blockers in mouse tumor models. *Oncimmunology* 2020;9:1721810.
- Liu P, Zhao L, Pol J, *et al*. Crizotinib-induced immunogenic cell death in non-small cell lung cancer. *Nat Commun* 2019;10:1486.
- Wang C, Wang J, Zhang X, *et al*. In situ formed reactive oxygen species-responsive scaffold with gemcitabine and checkpoint inhibitor for combination therapy. *Sci Transl Med* 2018;10:eaan3682.
- Finn RS, Ryou B-Y, Hsu C-H, *et al*. Tiragolumab in combination with atezolizumab and bevacizumab in patients with unresectable, locally advanced or metastatic hepatocellular carcinoma (MORPHEUS-Liver): a randomised, open-label, phase 1b-2, study. *Lancet Oncol* 2025;26:214–26.
- Chen Y, Jia K, Sun Y, *et al*. Predicting response to immunotherapy in gastric cancer via multi-dimensional analyses of the tumour immune microenvironment. *Nat Commun* 2022;13:4851.
- Liang H, Huang J, Li H, *et al*. Spatial proximity of CD8+ T cells to tumor cells predicts neoadjuvant therapy efficacy in breast cancer. *NPJ Breast Cancer* 2025;11:13.
- Rousalova I, Krepela E. Granzyme B-induced apoptosis in cancer cells and its regulation (review). *Int J Oncol* 2010;37:1361–78.
- Zhu X, Liang R, Lan T, *et al*. Tumor-associated macrophage-specific CD155 contributes to M2-phenotype transition, immunosuppression, and tumor progression in colorectal cancer. *J Immunother Cancer* 2022;10:e004219.
- Zhu Z, Zhang H, Chen B, *et al*. PD-L1-Mediated Immunosuppression in Glioblastoma Is Associated With the Infiltration and M2-Polarization of Tumor-Associated Macrophages. *Front Immunol* 2020;11:588552.
- Li W, Wu F, Zhao S, *et al*. Correlation between PD-1/PD-L1 expression and polarization in tumor-associated macrophages: A key player in tumor immunotherapy. *Cytokine Growth Factor Rev* 2022;67:49–57.
- Liu N, Zhang J, Yin M, *et al*. Inhibition of xCT suppresses the efficacy of anti-PD-1/L1 melanoma treatment through exosomal PD-L1-induced macrophage M2 polarization. *Mol Ther* 2021;29:2321–34.